JOURNAL OF GEOPHYSICAL RESEARCH, VOL. 105, NO. D1, PAGES 1537–1552, JANUARY 20, 2000

A Lagrangian view of stratospheric trace gas distributions

M. R. Schoeberl,[1] L. C. Sparling,[2] C. H. Jackman,[1] and E. L. Fleming[3]

Abstract. As a result of photochemistry, some relationship between the stratospheric age of air or mean age and the amount of tracer contained within an air sample is expected. The existence of such a relationship allows inferences about transport history to be made from observations of chemical tracers. This paper lays down the conceptual foundations for the relationship between age and tracer amount for long-lived tracers, developed within a Lagrangian framework. Although the photochemical loss depends not only on the age of the parcel but also on its path, we show that under the "average path approximation" that the path variations are less important than parcel age. The average path approximation then allows us to develop a formal relationship between the age spectrum and the tracer distribution. Using this relationship, tracer-tracer correlations can be interpreted as the result of mixing which connects parts of the "single-path photochemistry curve," a universal path-independent curve that describes the photochemical loss in terms of the total photon exposure. This geometric interpretation of mixing gives rise to constraints on trace gas correlation curves as can be seen in the atmospheric trace molecule spectroscopy observations.

1. Introduction

As air enters the tropical stratosphere, it moves upward and toward the extra tropics roughly along the streamlines of the Brewer-Dobson circulation. Mass balance requires that most of the air rising into the tropical stratosphere will immediately move poleward and subsequently descend into the middle world (see *Holton et al.*, [1995] for discussion of the middle world region of the stratosphere). However, some air continues to rise into the stratosphere and mix with the environment. Understanding the movement, residence time, and mixing of air within the stratosphere is key to assessing the impact of pollutants on the ozone layer.

The measurement of nearly inert trace gases, which have known time-dependent sources, can be used to estimate the time elapsed since the air first entered the stratosphere. This transit time is commonly called the mean age, and it gives important clues about the stratospheric circulation. The mean age depends not only on the timescale of the mean circulation but also on fluctuations around the mean transport; that is, it depends on the mixing. As we discuss below, the sampled air can have a complex time history; thus the transit time from the tropopause to some point within the stratosphere is not, in general, well-characterized by a single timescale.

The realization that the character of a sample of air is determined by both the transport and mixing history has led to the idea that the transit time is more aptly described by a distribution of timescales [*Kida*, 1983; *Hall and Plumb*, 1994]. In this distribution, each element corresponds to a single path connecting the source and observation or sample point. Thus an air sample can be considered to consist of a large number of "irreducible parcels," each of which has traveled along a single path that connects the source and the observation region at the time of the measurement. There are, of course, a very large number of such parcel paths, the maximum number being the number of molecules in the sample. One need not consider such a large number, however; the number of paths need only be chosen sufficiently large so that all the relevant ensemble statistics have converged. Increasing the number of parcels beyond this point will introduce no new information. Thus the sample consists of a statistically robust ensemble of irreducible parcels which have taken different paths to the sampling volume. The parcels are irreducible in the sense that whatever parcel splitting or stretching that occurs is implicitly accounted for by having a large number of parcels. The term parcel will here after refer to an irreducible parcel.

In terms of such an ensemble of paths the mean age can then be interpreted as the mean of the transit time distribution, commonly referred to as the "age spectrum" [*Hall and Plumb*, 1994] (hereinafter referred to as HP). Although it is easy to compute the age spectrum for a numerical model for which the mixing history is known, it is not possible to infer the age spectrum solely from observations. Given only an observation of the total amount of trace gas in the sample, we have no a priori knowledge of its detailed time history. Under some conditions, however, the mean age of a sample can be inferred from the amount of trace gas in the sample. Inferring the mean age becomes possible when there is something in the system that acts as a "clock," marking the passage of time along a parcel path from the source to the observation point. One example is an inert tracer with a monotonically increasing source $S(t)$ (HP). In this case, a parcel entering the stratosphere at time $t = t_o$ has mixing ratio $S(t_o)$ and is therefore tagged by its entry time.

Another example of a stratospheric clock occurs when the source is constant in time but the amount to trace gas in the parcel decays with time. In the simplest case the decay rate is independent of ambient conditions and is thus independent of path, for example, a radioactive tracer. In this simple situation, two parcels that take the same time to travel from the source

[1]NASA Goddard Space Flight Center, Greenbelt, Maryland.
[2]Joint Center for Earth Systems Technology, University of Maryland Baltimore County, Baltimore.
[3]Raytheon-STX, Laurel, Maryland.

Paper number 1999JD900787.
0148-0227/00/1999JD900787$09.00

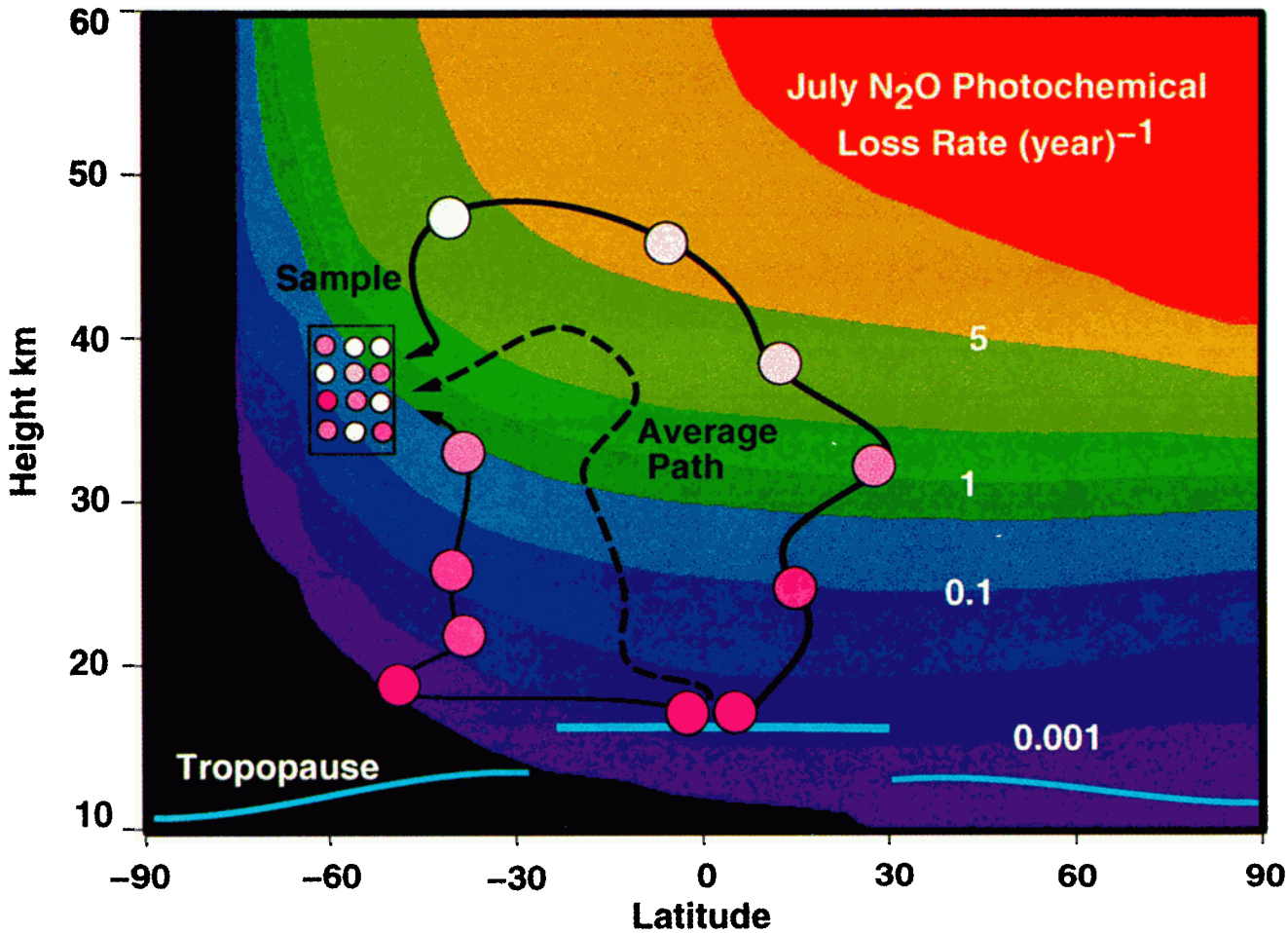

Plate 1. A cartoon showing the path of irreducible parcels to the sample point. Two parcel paths are indicated by arrows, the solid circles indicate the parcel trace gas amounts. The color fill indicates the amount of N_2O in each parcel, with darker color indicating a higher amount. The average path (average of many parcel paths) for parcels with the same age is shown by the dashed line. The background shows the loss rate (yr^{-1}) for N_2O. The cartoon illustrates the situation where two parcels having the same transit time to the sample point, nonetheless arrive with different amounts of N_2O. The horizontal lines indicate the tropopause.

to the observation point will have the same amount of tracer, even if they have traveled on different paths. This means that there is a 1:1 correspondence between the amount of trace gas in the parcel and the age of the parcel. The actual amount of a constituent measured in the sample is the volumetric average of the trace gas amounts of all parcels comprising the sample. Because there is a distribution of ages in the sample, there will also be a distribution of photochemical losses, and by analogy to the age probability distribution function (PDF) or "age spectrum," the distribution of trace gas amounts is the tracer PDF or "tracer spectrum."

In the case of stratospheric tracers such as N_2O or CH_4 the situation is more complicated. The amount of photochemical loss now depends on the accumulated exposure to photolyzing radiation or locally generated reactive compounds. For such "total exposure constituents" [*McIntyre*, 1992], the 1:1 relation between age and trace gas amount is blurred, and parcels with the same age may have different trace gas amounts, depending on the latitude and altitude range of their paths. This problem is illustrated in Plate 1. The cartoon shows two parcels that have the same age although they take different paths to arrive at the sample point with different N_2O amounts. This cartoon also illustrates the Lagrangian view of the mixing and transport process. The "sample" is the local assembly of irreducible parcels that have taken many different paths to the sample region. Because the parcels are irreducible, by definition, they do not mix with their environment on the way to the sample point.

As mentioned above, although we cannot directly observe the age spectrum in the real atmosphere, the age spectrum can be computed for a model. There are two methods. The first method is an Eulerian calculation. A pulse of inert tracer is released at the tropopause and allowed to disperse throughout the stratosphere. At a given point within the model domain the graph of the tracer amount versus time gives the age spectrum. Computing the age spectrum in this way is equivalent to finding the Green function solution to the model transport dynamics (HP) and assumes that nonstationary processes are negligible on the multiyear timescale of the problem. *Hall and Waugh* [1997] report the age spectrum and mean age distributions for two general circulation models using this method.

The second method is Lagrangian. A diabatic or kinematic trajectory model is used to move a large number of air parcels that are continuously released at the tropopause. After a long time (years) the age spectrum for a sample volume containing many parcels can be computed. No assumptions of stationarity

are made, which means that a trajectory computed age spectrum will vary in time. A further advantage of the trajectory method is the fact that Eulerian estimates of the mean age appear to depend on the advection scheme (J. Eluszkiewicz, personal communication, 1999), while the trajectory transport is nondispersive. The disadvantage of the trajectory method is that a very large number of parcels need to be used because the parcel density, similar to the atmospheric density, decreases exponentially with altitude.

The trajectory model method has an advantage in that it allows us to develop a Lagrangian interpretation of mixing and transport. For example, the observation that long-lived tracers are highly correlated, producing a compact relationship, has become an important tool in interpretation of stratospheric data. The formation of such a compact relationship is explained in a seminal paper by *Plumb and Ko* [1992] (hereinafter referred to as PK) using an Eulerian formulation. However, how do such compact tracer-tracer correlations develop from a Lagrangian viewpoint? A main goal of this paper is to demonstrate how tracer-tracer correlations can be understood within a Lagrangian framework.

In section 2 we develop the approximations that allow us to relate the tracer and age spectra and use some analytical and numerical examples to illustrate our concepts and to test the methodology. In section 3 we briefly discuss the age spectrum and the tracer PDF. In section 4 we extend the formalism to tracer-tracer correlations and show how such correlations can be interpreted within a Lagrangian framework. Section 5 summarizes the paper.

2. Photochemistry Along Lagrangian Paths

Following *Kida* [1983], *Plumb and McConalogue* [1988], HP, and *Hall and Waugh* [1997], we postulate, as discussed in section 1, that a "sample" of air contains a large number of irreducible parcels with different ages and composition. In the Lagrangian view, each of these irreducible parcels has traveled from the tropical tropopause (where we assume that all air enters the stratosphere) to a sample point as illustrated in Plate 1. Since these are irreducible parcels, mixing does not take place along the paths but is implied in the formation of the sample. The dependence of the total photochemical exposure on the parcel path gives rise to a distribution of trace gas amounts in the sample. In the following, we establish an approximate relation between the tracer and age distributions that follows from the fact that parcels with similar ages have similar photochemical exposures. This approximation allows us, in principle, to use photochemically active trace gases as markers of age.

The age spectrum $G_o(T, \mathbf{x}_s, \mathbf{x}_o)\, dT$ is the probability that the transit time from the source at $\mathbf{x}_o$ to the sample point $\mathbf{x}_s$ is in the range T to $T + dT$, and

$$\int_0^\infty G_o(T, \mathbf{x}_s, \mathbf{x}_o)\, dT = 1.$$

We identify $G_o(T, \mathbf{x}, \mathbf{x}_o)$ as the Green function for an inert tracer with a source $B_o(t, \mathbf{x}_o)$ at $\mathbf{x}_o$ such that the tracer concentration B_s at the sample point is

$$B_s(\mathbf{x}_s, \mathbf{x}_o, t) = \int_0^t B_o(T, \mathbf{x}_o) G_o(t - T, \mathbf{x}_s, \mathbf{x}_o)\, dT.$$

The sample mean age (HP) is

$$\Gamma = \int_0^\infty G_o(T, \mathbf{x}_s, \mathbf{x}_o) T\, dT.$$

For inert tracers with known time-dependent sources the mean age and the constituent amounts are directly related. With a linearly increasing inert tracer source, such as SF_6 or CO_2, $B_o(T, \mathbf{x}_o) \sim T$. Thus it is immediately obvious that the SF_6 or CO_2 amount will be proportional to the mean age (e.g., *Bischof et al.* [1985], *Schmidt and Khedim* [1991], and *Boering et al.*, 1996, for CO_2; *Elkins et al.* [1996], *Harnish et al.* [1966], and *Patra et al.* [1997] for SF_6).

Now we consider the case of a photochemically active tracer with a fixed tropopause mixing ratio. As mentioned earlier, the amount of tracer in each irreducible parcel depends on the path the irreducible parcels take to the sample point. Thus two parcels with the same age having different paths will very likely have different photochemical histories.

We assume that all air parcels are released at the tropical tropopause with constituent mixing ratio B_o which we take to be unity. The parcel i follows path $\mathbf{x}_i(t)$ and has a chemical loss rate $\beta[\mathbf{x}_i(t), t]$. The parcel amount of B_i is given by

$$DB_i/Dt = -\beta[\mathbf{x}_i(t), t]B_i, \tag{1}$$

where D indicates a Lagrangian (along path) derivative. Integrating (1) over the time T_i (the parcel age) it takes the parcel to arrive at the sample point, we obtain

$$\log (B_i) = -\int_0^{T_i} \beta[\mathbf{x}_i(t), t]\, dt = -T_i \bar{\beta}_i(T_i), \tag{2}$$

where

$$\bar{\beta}_i(T_i) = \frac{1}{T_i} \int_0^{T_i} \beta(\mathbf{x}_i(t), t)\, dt$$

and where the integration is over the ith parcel path. The overbar indicates the average over a single path. Let $P(B)$ be the distribution of tracer amounts within the sample, or the tracer spectrum. By analogy with the age spectrum the sample concentration is given by

$$B_s = \int_0^1 P(B) B\, dB, \tag{3}$$

where

$$P(B) = \int_0^\infty P(B, \mathbf{x}_s, \mathbf{x}_o \mid T) G_o(T, \mathbf{x}_s, \mathbf{x}_o)\, dT. \tag{4}$$

$P(B, \mathbf{x}_s, \mathbf{x}_o \mid T)$ is the conditional probability distribution of tracer amounts over the subset of irreducible parcels that have arrived at the sample point $\mathbf{x}_s$ at time T. To simplify the notation, we now suppress the explicit space dependence on the location of the sample point.

2.1. Tracers With Path-Independent Photochemical Loss

We first consider the simple example of a tracer released at the tropopause which has a path independent photochemical loss (like a radioactive tracer). For this tracer, $\beta_i = \beta =$

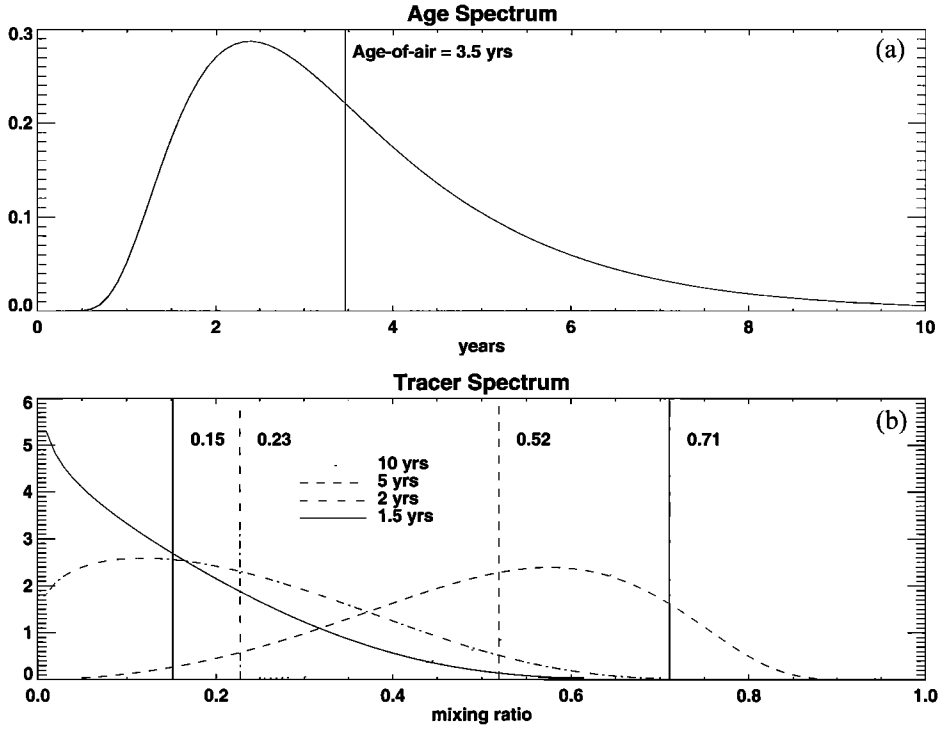

Figure 1. The age spectrum and the tracer spectrum are compared for tracers with different lifetimes. (a) Age spectrum using HP's analytical model (equation (8)), $K = 3.1$ m^2/s, $H = 7$ km, $z = 50$ km. (b) Corresponding tracer spectrum for trace gases with different lifetimes, β^{-1}, in equation (9). The vertical lines show the first moment of each distribution. In Figure 1a the first moment is the mean age, while in Figure 1b the first moments are the mixing ratios for the sample with the assumed bottom boundary value of 1.0.

constant, and the loss along the path is simply $B = e^{-\beta T}$. Since there is now a one to one relation between B and T,

$$P(B \mid T) = \delta(B - e^{-\beta T}). \tag{5}$$

Substituting (5) into (4) gives

$$P(B) = \int_0^\infty \delta(B - e^{-\beta T}) G_o(T)\, dT = \frac{1}{\beta B} G_o[-\log (B^{1/\beta})]. \tag{6}$$

Equation (3) can be written as

$$B_s = \int_0^\infty G_o(T) e^{-\beta T}\, dT \equiv \tilde{G}_o(\beta), \tag{7}$$

where $\tilde{G}_o(\beta)$ is the Laplace transform of the age spectrum.

Let us now extend the example using the analytic age spectrum from the one-dimensional (1-D) diffusion model as developed by HP. The HP age spectrum is given by

$$G_o(z, T) = \frac{z}{2\sqrt{\pi K T^3}} \exp\left[-(z/\sqrt{4KT} - \sqrt{KT}/2H)^2\right], \tag{8}$$

where K is the diffusion coefficient, H is the atmospheric scale height, and z is the height. Despite its simplicity, this age spectrum (equation (8)) has many characteristics of more realistic age spectra produced by 3-D and 2-D transport models. The Laplace transform of (8) is

$$\tilde{G}_o(\beta, z) = \exp\left(\frac{z}{2H} - \frac{z}{2H}\sqrt{1 + 4\beta H^2/K}\right). \tag{9}$$

Figure 1 shows the age spectrum and four corresponding tracer spectra, $P(B)$, for different values of β using (9). For short-lived tracers the tracer spectrum is quite broad, reflecting the spread in tracer values within the sample due to photochemistry. For very fast photochemistry a large number of parcels have zero tracer content and the distribution "piles up" on the left-hand side of Figure 1. On the other hand, for an inert tracer the tracer spectrum is a δ function, $\delta(B_s - B_o)$ (not shown).

For long-lived tracers, $4\beta H^2/K \ll 1$, then (9) becomes

$$B_s \approx \exp(-z\beta H/K) = \exp(-\beta\Gamma),$$

or

$$\Gamma \approx -\log(B_s)/\beta, \tag{10}$$

as might be expected. (Note that the quantity $4H^2/K \approx 2$ years for $K = 3.1$ m^2/s (HP), $H = 7$ km as used in Figure 1; thus $1/\beta \gg 2$ years).

Sometimes a supposedly inert tracer is found to have a weak photochemical loss. The effect of this photochemistry is to shift the estimated mean age computed by the stratosphere-troposphere lag method toward older values [*Hall and Waugh*, 1998]. For a tracer with a linearly increasing source the lag-computed "age" is given by $\Gamma_s = (B_o - B_s)/R$, where R is the tropospheric rate of increase of the tracer, $B_o = Rt$, with $B_o(t < 0) = 0$. Now, following *Hall and Waugh* [1998], we compute the age if there is some loss. The stratospheric value of the tracer for this time dependent source is

$$B_S = \int_0^\infty G_o(T)e^{-\beta T}(t - T)R\, dT = Rt\tilde{G}_o(\beta)$$

$$- R\int_0^\infty G_o(T)e^{-\beta T}T\, dT$$

$$= Rt\tilde{G}_o(\beta) + R\frac{\partial}{\partial\beta}[\tilde{G}_o(\beta)]. \quad (11)$$

Using (11), we obtain the age,

$$\Gamma_s = t[1 - \tilde{G}_o(\beta)] - \frac{\partial}{\partial\beta}\tilde{G}_o(\beta). \quad (12)$$

This expression is equivalent to *Hall and Waugh*'s [1998] equation (A5). To see that Γ_s is always greater than Γ for $t > \Gamma$, consider a δ function age spectrum, $G_o(T, \mathbf{x}, \mathbf{x}_o) = \delta(T - \Gamma)$, as might be produced by purely advective transport. Then $\tilde{G}_o(\beta) = e^{-\beta\Gamma}$ and (12) becomes

$$\Gamma_s \approx \Gamma[1 + \beta(t - \Gamma)]. \quad (13)$$

As noted by *Hall and Waugh* [1998], the lag-computed age increases with time when the tracer has some loss because the stratospheric rate of tracer increase does not keep up with the tropospheric rate of tracer increase.

2.2. Photochemically Active Tracers

For most trace gases of interest the loss rate is not constant so the relation between the age spectrum to the tracer spectrum is not straightforward. However, (3) and (4) can be generalized to include photochemical processes that are path-dependent. Although the time dependence is not explicitly included in the derivation below, the effects of time dependence on the photochemical loss rates will be assumed to be small because the integration over long paths effectively integrates over diurnal and seasonal variations in photochemical loss.

From (2), (3), and (4),

$$B_s = \int_0^\infty G_o(T)\langle e^{-\bar{\beta}_t(T)T}\rangle\, dT, \quad (14)$$

where

$$\langle e^{-\bar{\beta}_t(T)T}\rangle = \int_0^1 B_t P(B_t \mid T)\, dB_t$$

and angle brackets indicate the ensemble average over all paths of age T.

Now consider the average photochemical loss rate averaged over paths with age T, $\langle\bar{\beta}(T)\rangle$, and assume that the deviations from this average loss rate are small. Thus we assume that $\bar{\beta}_t(T) = \langle\bar{\beta}(T)\rangle + \overline{\delta\beta}_t(T)$, where $\langle\overline{\delta\beta}_t(T)\rangle = 0$ and $\overline{\delta\beta}_t(T)/\langle\bar{\beta}(T)\rangle \ll 1$. Then,

$$\int_0^\infty G_o(T)\langle e^{-\bar{\beta}_t(T)T}\rangle\, dT = \int_0^\infty G_o(T)e^{-\langle\bar{\beta}(T)\rangle T}\langle e^{-\delta\beta_t(T)T}\rangle\, dT$$

$$= \int_0^\infty G_o(T)e^{-\langle\bar{\beta}(T)\rangle T}\langle 1 - \delta\beta_t(T)T + [\delta\beta_t(T)T]^2/2 \cdots\rangle\, dT. \quad (15)$$

The second term in the Taylor expansion vanishes identically, and we note that most of the contribution to the integral comes from times $T \le 1/\langle\bar{\beta}(T)\rangle$ so that for large T the high-order terms vanish. Thus (14) becomes

$$B_s \approx \int_0^\infty G_o \exp(-\langle\bar{\beta}(T)\rangle T)\, dT, \quad (16a)$$

which is essentially equivalent to the approximation

$$\langle\exp[-\bar{\beta}_t(T)T]\rangle \approx \exp[-\langle\bar{\beta}(T)\rangle T]. \quad (16b)$$

As we show in section 2.3, (16) turns out to be a good approximation for most long-lived trace gases with tropospheric sources. Thus the truncation of the Taylor expansion in (15) appears justified [see also *Volk et al.*, 1997]. For parcels with high age values, or parcels in the vicinity of strong photochemical gradients, we have found that there is a much greater dispersion in photochemical exposure so $\delta\beta_t(T)$ can be quite large and the approximation breaks down. However, for the older parcels the photochemistry reduces the constituent amounts so much that variations in photochemical exposure are often irrelevant.

Equation (16) now allows us to make the same direct connection between the age spectrum and the tracer spectrum that we exploited in the case of the radioactive tracer. We now turn to the problem of computing $\langle\bar{\beta}(T)\rangle$. To the same order of approximation, $\langle\bar{\beta}_t[\mathbf{x}_t(T)]\rangle \approx \bar{\beta}[\langle\mathbf{x}(T)\rangle]$, where $\langle\mathbf{x}(T)\rangle$ is the average path of duration T from the source position $\mathbf{x}_o$ to the sample position $\mathbf{x}_t$. The "average path approximation" (APA) works because the variability in photochemical loss is usually not a strong function of meridional position (see Plate 1) except across the polar vortex boundary. In the vortex boundary region, both the meridional excursions are large and the photochemical loss rate varies rapidly so APA will probably not work well.

2.3. Numerical Model

To further explore the theoretical model and approximations developed above, we use a 2-D trajectory model which utilizes the residual circulation and mixing coefficients of the 2-D chemical model of *Jackman et al.* [1996]. The residual circulation is computed from diabatic heating rates. To simulate mixing, we scramble the vertical and horizontal parcel positions at each time step by length, $L = R\sqrt{K\Delta t}$ [*Feller*, 1968], where R is a random number which takes the values -1 or 1. K is K_{yy} or K_{zz} in the usual notation. We tested this procedure by computing K_{yy} from parcel dispersion using

$$K_{yy} = \frac{1}{2}\frac{\partial\langle y^2\rangle}{\partial t},$$

where y is N-S distance [*Kida*, 1983] and confirming that the diagnosed K_{yy} was equal to the 2-D model K_{yy}.

The advantage of using the 2-D trajectory model compared to a 3-D trajectory model is that the faster interpolation and lower memory requirements of the 2-D model permit fast multiyear integration for a very large number of parcels. The 2-D trajectory model is ~100 times faster than the 3-D model. The mean age distribution for the 2-D model [*Fleming et al.*, 1999] agrees reasonably well with aircraft observations reported by *Waugh et al.* [1997b], and parcel spectra from long runs of a 3-D trajectory model are very similar to the spectra from the 2-D model.

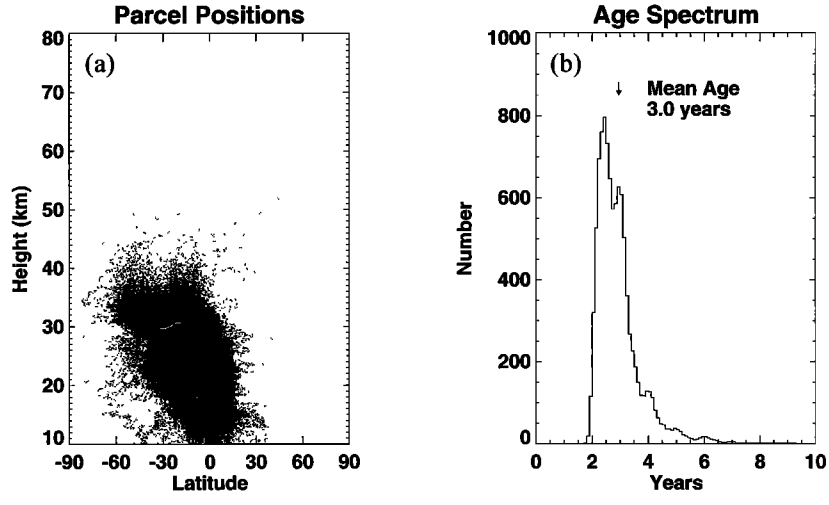

Figure 2. (a) Back trajectories positions from a regular array of 10,000 starting points in a 1 km by 1° latitude grid box at 35°S latitude and 30 km. The parcel positions are plotted every 3.6 days and appear as a dark cloud of points surrounding the average path (white line). (b) The age spectrum for the grid box. The age for each parcel is the time required for the parcel to descend to 2 km.

Figure 2a shows model back trajectories for 10,000 parcels uniformly placed in a 1° latitude by 1 km altitude sample domain at 35°S and 30 km. Parcels are integrated backward for 10 years. The parcel age is defined here as the time it takes for a parcel to move on a backward trajectory from the sample point to below 2 km in altitude. In Figure 2a, parcel position points along each path are plotted every 3.6 days down to 10 km altitude; the average path for all the parcels is also shown as the white line. The average path is computed by averaging all parcel x and y positions at each backward step down to the tropical tropopause. Figure 2a shows that the highest parcel density is close to the average path, although there are some wide excursions for the oldest parcels.

The age PDF for the calculation shown in Figure 2a is shown in Figure 2b. The minimum age of any parcel is ~2 years. Starting after 2 years, the age PDF generally resembles the age spectrum for the HP diffusion model (equation (8)) as well as the age spectra for most 3-D and 2-D models [*Waugh et al.*, 1997b; *Hall et al.*, 1999].

As an aside, it is interesting to compare the mean age for the 2-D model using the Lagrangian and Eulerian methods. This comparison provides a further check on the quality of the trajectory calculations. Plate 2a shows the 2-D model mean age computed using the Eulerian method. Plates 2b and 2c show the January 1, Lagrangian computed mean age with and without mixing, respectively. The Lagrangian calculation with mixing is performed using 1° by 1 km, sample regions (like that shown in Plate 3a) located on the 2-D model grid points. From each of the sample regions, 400 parcels were run backward for 20 years. To show the effect of mixing on the mean age (Plate 2c), the parcel calculation shown in Plate 2b is rerun with $K_{yy} = K_{zz} = 0$ above 10 km. If there is no mixing, the age spectrum for each sample box is very narrowly peaked. (It is not a δ function because there is mixing within the troposphere). We thus were able to estimate the mean age using a higher resolution 2 km by 2° grid of sample boxes containing only a few parcels per sample box for Plate 2c. Because the 2-D model circulation has stagnation points, occasionally a parcel will be trapped in the stratosphere. This gives rise to the five small spots of very old air seen in Plate 2c.

Although the mean age distributions shown in Plates 2a and 2b are in general agreement, there are some interesting and not completely explained differences between the trajectory mean age calculation and the Eulerian mean age calculation. For example, the Eulerian calculation shows older air at high latitudes and altitudes compared the trajectory-computed age. We have not found a precise explanation for this difference.

The trajectory mean age calculation also shows more descent at the South Pole than at the North Pole which is opposite to the Eulerian computed mean age. This difference arises from the fact that the Eulerian method averages over seasonal fluctuations in transport, while the trajectory method produces an instantaneous mean age distribution for January 1. The trajectory model is exhibiting the remains of the strong south polar descent of old air from the upper stratosphere, while the Eulerian calculation shows the seasonal average of descent over both poles. We also note that the tropical upwelling zone of young air is quite narrow in Plate 2a but is comparatively broad on the northward tropical flank in Plate 2b. This is also characteristic of a seasonal averaging in Plate 2a. The calculation shown in Plate 2c gives similar results to Plate 2b except that the air outside the tropical lower stratosphere is everywhere younger than that shown in Plate 2b. The increase in mean age from Plates 2b to 2c occurs because path lengths are always longer when random walks are included.

The comparison of the mean age calculations is not directly relevant to this study, but it does highlight an important issue relative to Lagrangian and Eulerian transport methods, namely, that Lagrangian and Eulerian transport calculations, in general, do not exactly agree. The differences between the two calculations are probably due to numerical effects associated with the Eulerian transport schemes (J. Eluszkiewicz, personal communication, 1999) but this issue needs further exploration.

Using the 2-D trajectory results shown in Figure 2, we can test the approximation (16) and APA. We use the annually averaged N_2O loss rates from the 2-D model and compute the N_2O amount for each parcel starting with the tropical tropopause amount as the initial condition. Figure 3a shows the scatter plot of parcel ages versus N_2O amount. There is a fairly

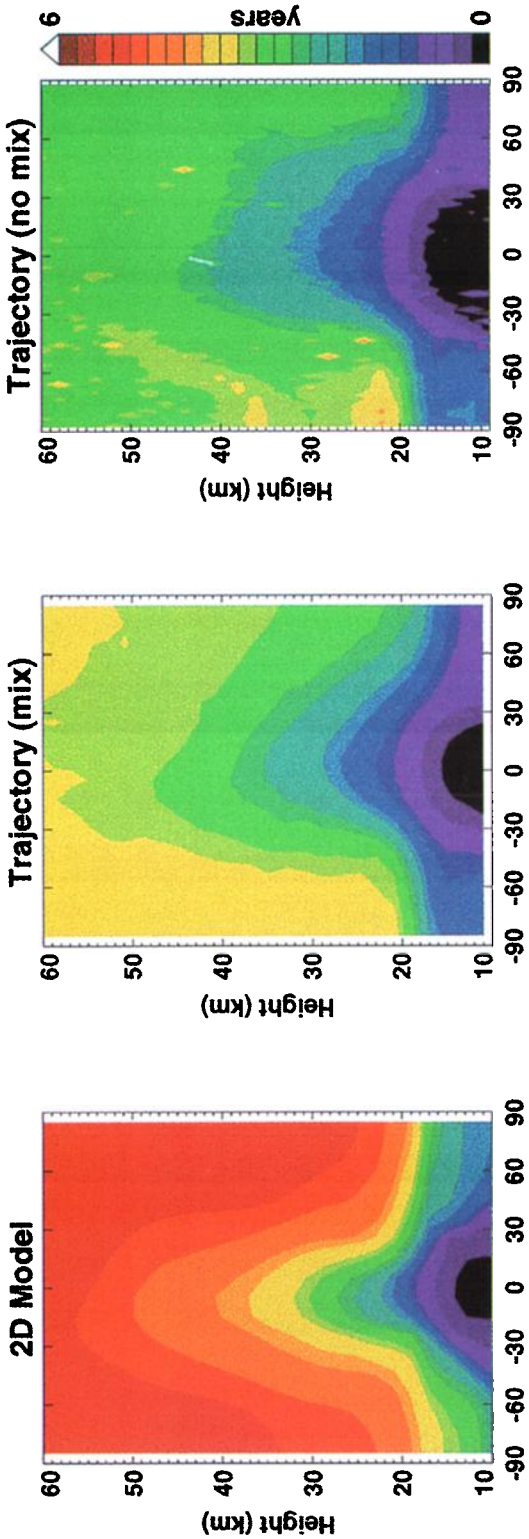

Plate 2. (a) Mean age for the 2-D model computed using the Eulerian method. (c) Mean age computed using back trajectories. The age spectrum is computed using 400 parcels contained within a 1 km by 1° grid box centered at each of the 2-D model grid points (see Plate 3a for grid box positions). The age of air is then computed from the spectrum. Mixing is included (see text). (c) Mean age computed from back trajectories using a uniform 2 km by 2° grid over the domain. Mixing is not included.

clear correlation between tracer amount and age but a noticeable increase in the scatter with increasing age. The increase in scatter with age results from the wider range in photochemical exposure experienced by the older parcels. Figure 3b shows the parcel paths for some selected parcel ages. The average path for each group of parcels is shown with the shaded line. The approximation (equation (16b)) basically assumes that we can replace the chemical effects of averaging over all the paths in each age bin by the chemistry taking place over the average path.

Figure 4a shows the tracer spectrum and mean tracer value normalized by the tropical tropopause value. The spectrum looks similar to the tracer spectra shown in Figure 1 for the (5 year)$^{-1}$ loss rate but also shows the statistical pile up at low tracer amounts seen in the short lifetime case shown in Figure 1. The statistical pile up near zero is due to the long transit time parcels that have had high total photochemical exposure.

To test the approximation (16b), we compute the averaged photochemical loss for each of the paths in a 0.1-year age bin and compare the result to the loss computed using the average path for each age bin (see Figure 3b). Figure 4b shows the parcel average loss amount versus age (left-hand side of (16b)) compared to the value estimated using APA (right-hand side of (16b)) also shown are the loss amounts for the individual parcels sorted by age (dots). Figure 4b shows that (16b) is an excellent approximation for ages up to 4 years and seems to be a reasonable approximation even for ages beyond 4 years where comparisons are more difficult because of fewer parcels. (There are no values below 2 years as indicated in Figure 2b). Figure 4c shows the original age PDF and the integrand of (16a), the modified PDF, using APA and the exact loss amounts shown in Figure 4b. Figure 4b shows that even though APA is less accurate for ages greater than roughly 4 years, the effect on the modified PDF is negligible because the amount of tracer is greatly reduced at large times.

Plate 3 shows the extension of the results shown in Figures 3 and 4 to the whole stratosphere except only 2000 parcels are used for each sample. Using the annual average photochemical loss rates, the N_2O amount is computed from individual parcel trajectories and APA for each of the sample boxes shown in Plate 3a, which also shows the mean age (same as Plate 2a). For each sample region 2000 parcels are used. The N_2O distributions obtained using all of the trajectories and using APA are shown in Plates 3a and 3b, respectively. In general, the differences between the exact and APA are small, consistent with the results we expect from Figure 4b. Closer examination (Plate 3c) shows that exact distribution has a somewhat steeper vertical gradient with altitude than the APA computation. This is understandable since APA will tend to underestimate the contributions of longer paths. We have also computed the percentage differences between the exact N_2O and the APA computed amount. For N_2O values >30 ppbv, the differences are <10%. For smaller N_2O values the differences are below 30% except within the polar vortex where the differences can rise to 70%. Plate 3d shows the sample N_2O amount (for both APA and exactly computed trace gas amounts) plotted against the mean age for each of the sample boxes shown in Plate 3a. The sample mean age and trace gas amount are correlated, but there is significant scatter. The scatter occurs because of variations in the age spectrum between samples with the same mean age. This result shows that mean age is not always a good predictor of the tracer amounts because the tracer amount is

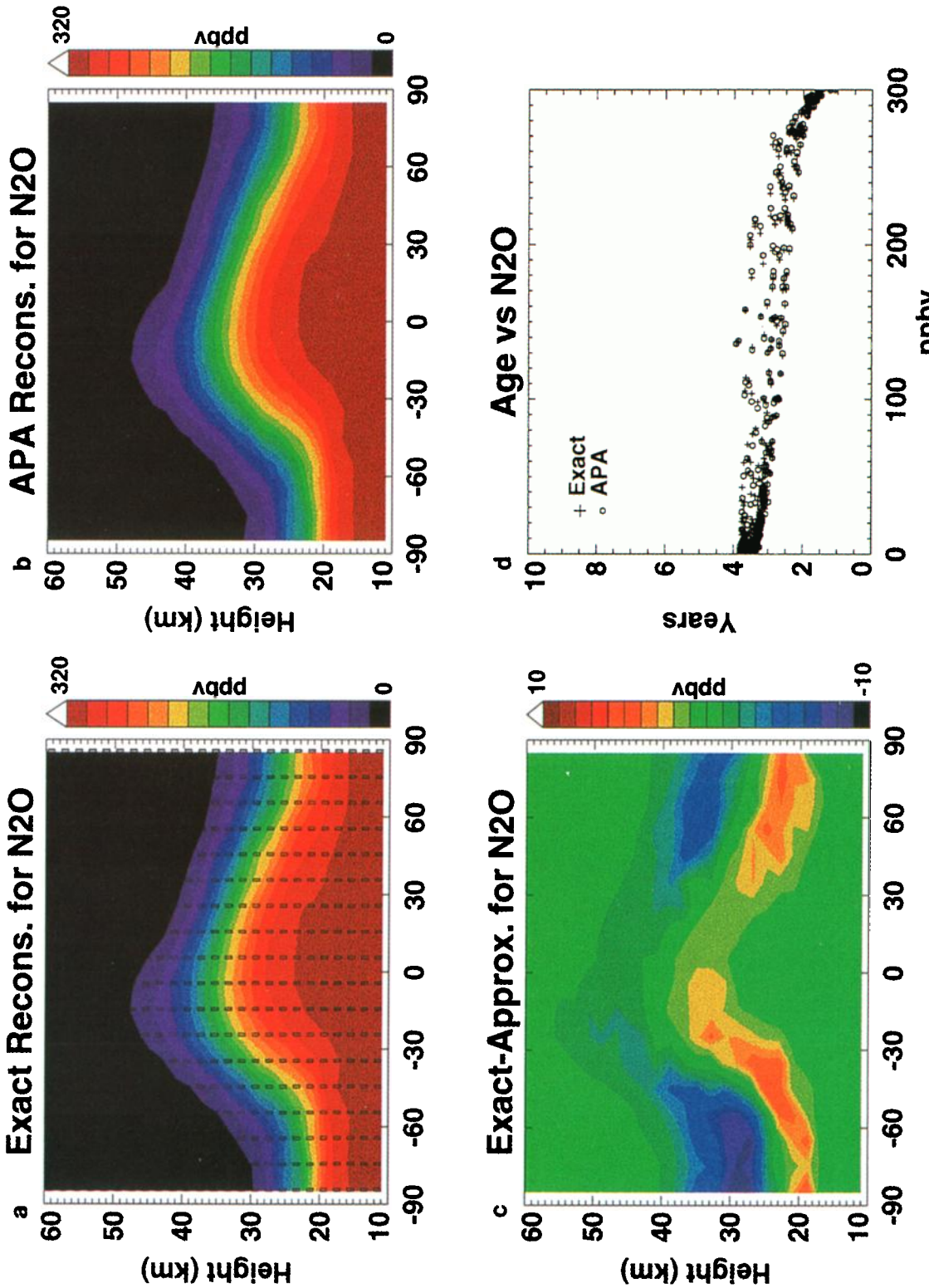

Plate 3. (a) The N_2O distribution for each grid box computed by integrating over each path and using the annually averaged loss rate from the 2-D model. Grid box positions are shown; 2000 parcels were used for each sample box. (b) The N_2O distribution reconstructed using APA. (c) Difference between Plates 3a and 3b. (d) Plot of sample mean age versus N_2O amount for all of the sample boxes shown in Plates 3a and 3b.

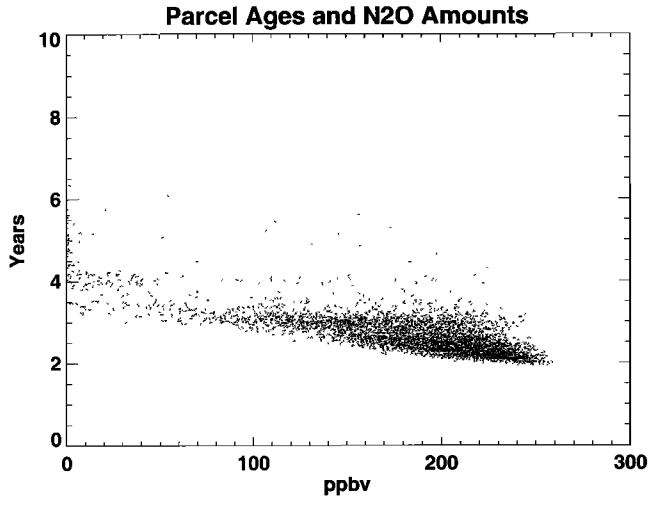

Figure 3a. A scatterplot of N_2O versus age for the 10,000 parcels shown in Figure 2.

determined by the younger part of the age spectrum rather than whole spectrum.

3. Age Spectrum and Tracer Samples

The relationship between the age or tracer spectrum associated with a given sample and the PDF of many samples is not straightforward since the same mean tracer value can be produced from different tracer spectra. However, there are some obvious relationships that can be exploited. If multiple tracer measurements are made, we can write (16a) in discretized form as

$$B_k = \sum_k \sum_j \exp\left[-\langle \bar{\beta}_{k,j}(j\Delta t)\rangle j\Delta t\right] G_o(j\Delta t)\Delta t,$$

where k indicates each tracer and $j\Delta t$ is the age. In matrix form this equation is $\mathbf{B} = \mathbf{L}\mathbf{G}_o$ where the matrix $L_{k,j} = \exp(-\beta_{k,j}j\Delta t)\Delta t$. The age spectrum can now be determined by the matrix equation

$$\mathbf{G}_o = \mathbf{L}^{-1}\mathbf{B}. \tag{17}$$

Since $\mathbf{L}$ must be square, (17) shows that the measurement of N tracers, each having a different chemical loss rate, allows us to obtain N pieces of information about the age spectrum. It is also obvious that N tracer measurements can uniquely define the age spectrum. A corollary to this statement is that the age spectrum cannot change along the surface of common tracer isopleths. For example, let us say that measurements of methane, N_2O, SF_6, CO_2, etc., have a constant mixing ratio along some surface, then that mixing ratio surface is also a surface where the age spectrum is fixed.

It is important to understand the difference between a single tracer spectrum and the PDF generated from many samples. To illustrate this difference, consider a well-mixed atmosphere.

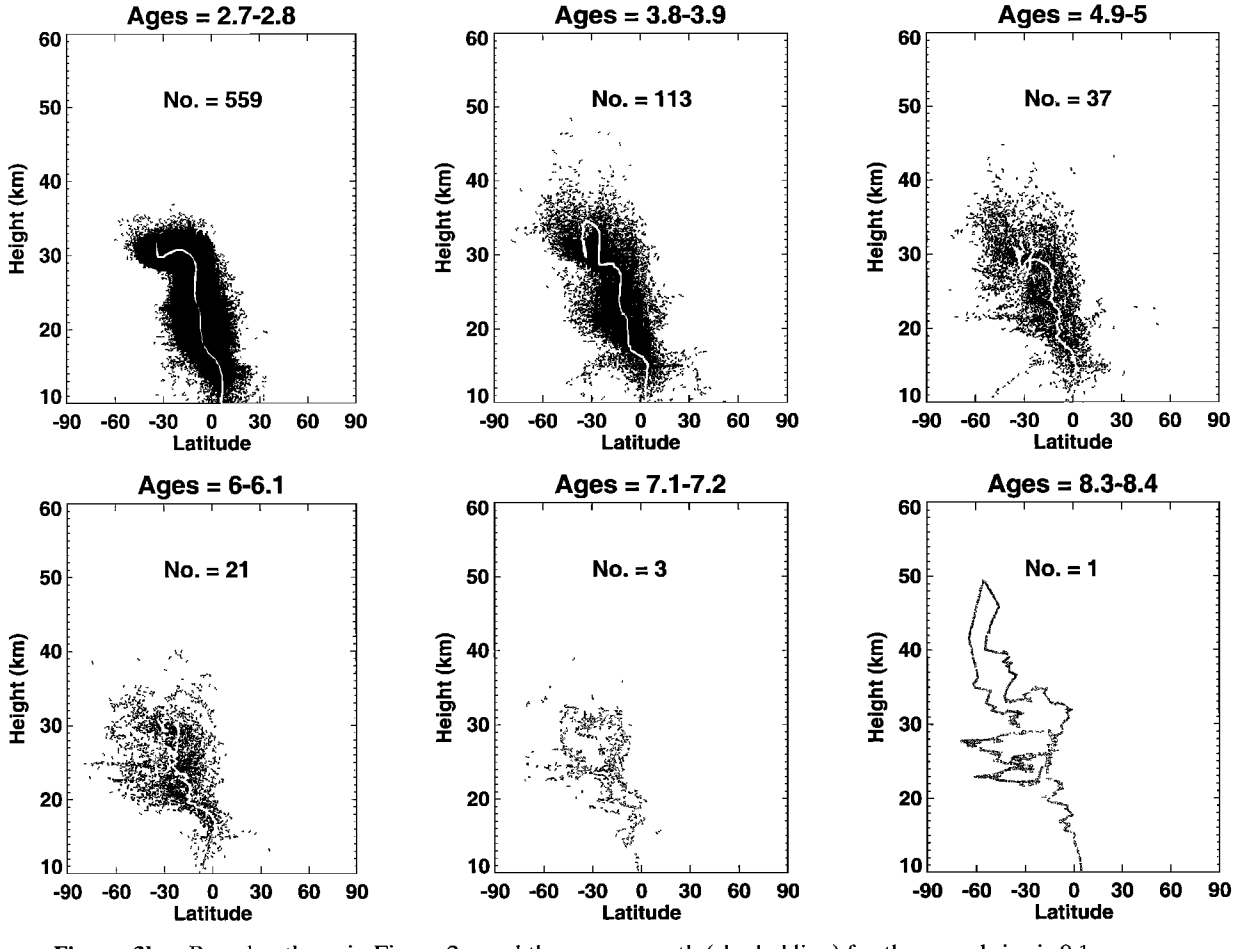

Figure 3b. Parcel paths as in Figure 2a, and the average path (shaded line) for the parcels in six 0.1-year age bins.

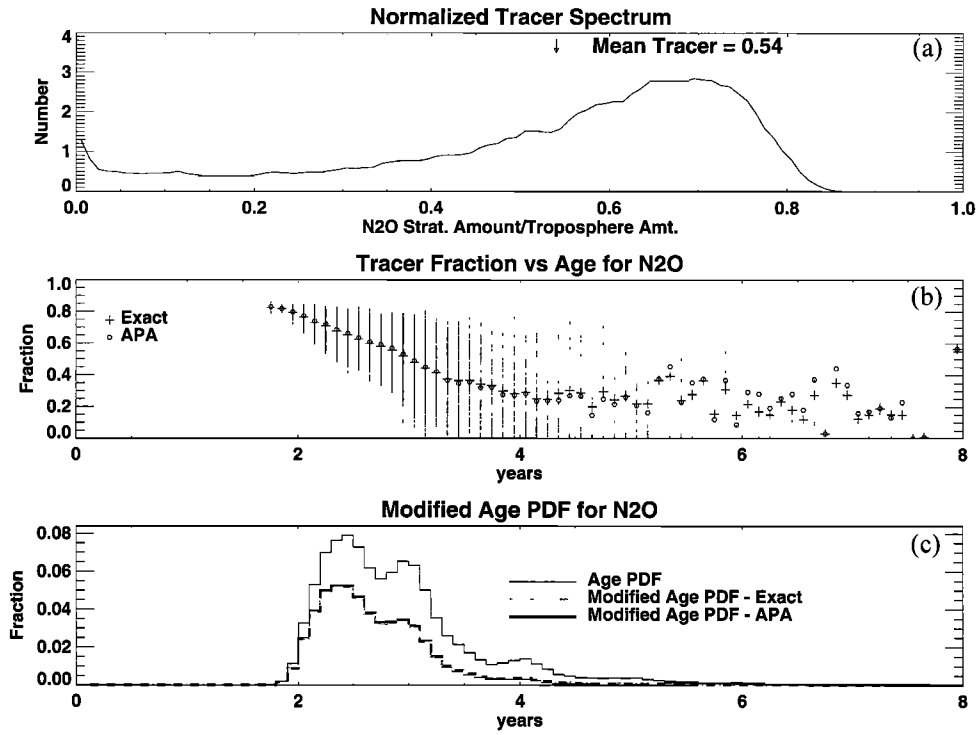

Figure 4. (a) The normalized N_2O tracer spectrum with the mean value indicated. The N_2O tracer amount is divided by the tropopause value. (b) A comparison of tracer fraction verses age for N_2O. Crosses indicate the average tracer fraction computed by integrating all the parcel back trajectories with the same age. Each parcel fraction is shown as a small dot. The solid circles show the results obtained from using APA for each age bin. (c) The age PDF (thin line) multiplied by the tracer fraction for each age (thick shaded dashed line) shown in Figure 4a. The thick solid line shows the results using APA. The two thick lines lie nearly on top of each other.

By definition, all the trace gas samples will have the same mixing ratio so the PDF made from many different samples will be a delta function. The tracer spectra will also be the same for each of the samples (a result from the preceding paragraph), but the tracer spectra may not be a δ function; in fact, it is more likely that the tracer spectrum will be broad and flat. The opposite may be true if the sample PDF is broad, which indicates that the samples have quite different trace gas values. A way to achieve this type of sample PDF is for the individual tracer spectra to be sharply peaked with different first moments. These examples show that the tracer spectra and the tracer PDF can exhibit quite different, even opposite, behavior.

More realistically, we can think of three distinct atmospheric regions in the lower stratosphere: The first is the tropics where air has entered the stratosphere and is relatively young. The second is the winter polar region, where air has descended from the upper stratosphere and is relatively old. The third is the midlatitude region, where air is mixing between the polar and tropical region. In the case of photochemically destroyed gases released at the tropopause, as we move from the tropical to the polar regions we expect a continuous shift in the first moment of the tracer spectrum toward smaller trace gas values. The tracer PDF obtained from many samples, on the other hand, will show at least three distinct peaks in winter associated with the three regions.

4. Tracer-Tracer Correlations

Tracer-tracer correlations have emerged as an important tool for unraveling physical processes within the stratosphere. The strong correlations between various long-lived tracers has been explained by PK as a consequence of rapid isentropic mixing combined with the large-scale overturning circulation. In this section, we extend the Lagrangian approach to include tracer-tracer correlations.

Plate 4 shows a cartoon of the atmospheric sampling and analysis process. In Plate 4, an aircraft samples air with different ages and different tracer amounts, as indicated by the colored dots. Isochrons, or equal mean age isopleths, are indicated by the green contours. On a tracer-tracer diagram, the sample trace gas amounts are plotted. Each sample consists of a large number of irreducible parcels, which are characterized by the age spectrum $G(t)$. Each of the irreducible parcels contains some amount of trace gas determined by the parcel's photochemical exposure, which has reduced, in the case of Plate 1, the trace gas from its tropopause value. The photolysis rate is $J_B = \int \sigma_B F \, d\lambda$, where σ_B is the absorption cross section of tracer B and F is the radiative flux. Both F and σ_B are functions of the wavelength λ. It turns out that the photolysis cross sections for many of the long-lived tracers have similar functional form [*DeMore et al.*, 1994] so we can write $J_B \approx \beta_B \int \sigma F \, d\lambda$, where β_B is a constant. Now defining the photochemical exposure n, where $dn = (\int \sigma F \, d\lambda) \, dt$, we can write for parcel i,

$$\log (B_i) = -\beta_B n. \tag{18}$$

Note the similarity between (18) and (2). Of course, the photochemical exposure is only approximately related to actual time because of the variations in photochemical loss rates with

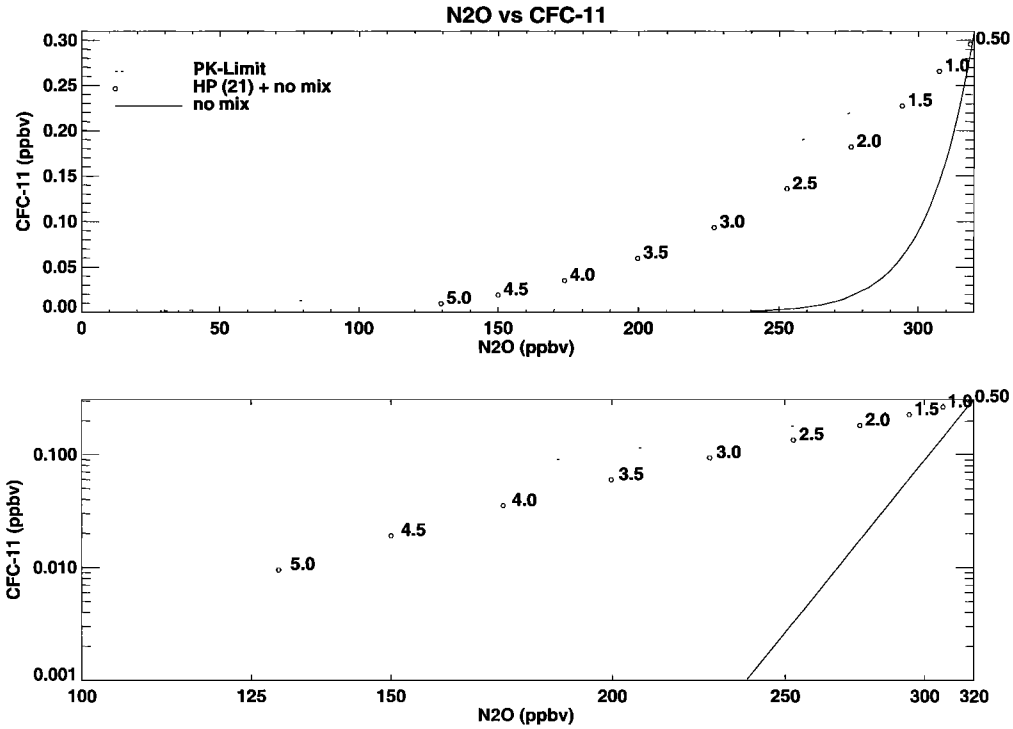

Figure 5. (top) The solid line shows N_2O versus CFC-11 using each of the chemical trajectory values. The mixing of the Lagrangian points according to the age spectrum (10) form the circles. The numbers next to each circle indicate the mean age. The dotted line is the PK-limit curve defined using the global lifetime of the two tracers from the 2-D model and equation (19). (bottom) The same diagram using the log of the mixing ratio.

altitude and latitude. We now consider a second trace gas, A, with $n = -\log(A_i)/\beta_A$. Eliminating n gives

$$A_i = B_i^{\beta_A/\beta_B}. \tag{19}$$

As a parcel moves through the stratosphere, the amounts of A_i and B_i in the parcel trace the "single-path photochemistry curve" (SPPC) shown in Plate 4. Even though individual irreducible parcels will trace approximately the same curve, the individual parcels composing the sample will end up at different points on the SPPC as a result of their different photon exposure. The actual tracer amount in the sample is then determined by the distribution, $G_o(T)$, of the irreducible parcels along the SPPC curve. Plate 4 (bottom) illustrates the weighting of the irreducible parcels by $G_o(T)$.

In the more general case the tracer photolysis cross sections can have different functional form

$$\log(A_i) = \int \frac{\beta_A}{\beta_B} d[\log(B_i)], \tag{20}$$

where the integration takes place over the parcel path and β is now the photochemical loss coefficient. Using (16),

$$A_s = \int_0^\infty A_i(T) G_o(T)\, dT = \int_0^\infty B_i^{\langle\beta_A(T)\rangle/\langle\beta_B(T)\rangle} G_o(T)\, dT. \tag{21}$$

To better illustrate (21), we consider two simple examples. In the first example the sample consists of two equal numbers of irreducible parcels that have ages T_1 and T_2. Then $G_o(T) = [\delta(T - T_1) + \delta(T - T_2)]/2$, $\Gamma = (T_1 + T_2)/2$, $B_s = (B_1 + B_2)/2$, and $A_s = (B_1^{\beta_A(T_1)/\beta_B(T_1)} + B_2^{\beta_A(T_2)/\beta_B(T_2)})/2$. The sample point (A_s, B_s) lies at the midpoint of a chord that intersects the curve at (A_1, B_1) and (A_2, B_2). In general, for a SPPC curve whose curvature does not change sign over the domain, mixing will produce sample points on the interior side of the curve. All sample points must obviously lie below the chord connecting (1, 1) and (0, 0), the limit chord, and above the SPPC. This result can be demonstrated by considering trace gas amounts from the groups (1, 1) and (0, 0) and by adjusting the fraction in each group continuously.

In the second example we use the age spectrum from HP (equation (8)). For a radioactive-type tracer the trace gas amount is given by (9). With a little algebra it is easy to show that

$$A_s = B_s^{(1-\sqrt{1+4\beta_A H^2/K})/(1-\sqrt{1+4\beta_B H^2/K})}. \tag{22}$$

In the limit of long-lived tracers, (22) has the same form as (19), which recovers the result first derived by PK for the global diffuser model. In the other extreme case where the tracer is short lived, $2H\sqrt{\beta/K} \gg 1$, (22) becomes, $A_s \approx B_s^{\sqrt{\beta_A/\beta_B}}$. This function is not as curved as the SPPC because the weighting function $G_o(T)$ averages over the more steeply curved SPPC function thus producing a shallower curve. These results reinforce the notion that the relationship between the tracers given by PK (their equation (13)) applies to tracers whose lifetime is long compared to the mixing time.

To generate an even more realistic picture of tracer-tracer correlation, we use values of $\bar{\beta}_A$ and $\bar{\beta}_B$ from the 2-D model using N_2O and CFC-11 loss rates for March. In this experiment we continuously release parcels at the tropical tropopause for 20 years and track their chemical composition. Parcels entering the troposphere are removed. At steady state, there are about

260,000 parcels in the stratosphere. The loss rates as a function of parcel age are generated using APA by sorting the trajectories by age and then averaging, $\langle\bar{\beta}_A\rangle = \log(A_o/A)/T$, $\langle\bar{\beta}_B\rangle = \log(B_o/B)/T$ within an age bin, where A_o, B_o are tracer values at the tropopause.

Figure 5 shows linear and log plots of CFC-11 versus N_2O computed from the trajectory model. The SPPC curve shows the composition of the individual parcels. The log plot of the trace gas amounts demonstrates the prediction of an exponential form as suggested by (19). Sample trace gas values are computed using $G_o(T)$ from (8). Increasing the mean age Γ (by increasing z in (8)) extends the age spectrum. Substituting (8) into (21) and varying z, we produce the points shown in Figure 5 labeled with the age in years. The linear relationship between $\log(A)$ and $\log(B)$ is predicted by (20).

Let us reverse the procedure and take the 2-D chemical model global lifetimes as an estimate of $\langle\beta_A\rangle$ and $\langle\beta_B\rangle$ to generate a curve from (19). The global lifetime is the ratio of the total stratospheric tracer amount to the cross tropopause tracer flux. The 2-D chemical model global lifetime is 117.8 years for N_2O and 51.6 years for CFC-11. Using the inverse lifetimes as the loss rates, we generate the dashed curve in Figure 5. This curve can be thought of as an upper bound on the mixing in the 2-D model. We refer to this upper bound as the PK-limit since (19) has the form of PK's equation (15) for this case. The PK limit is below the limit chord (which is not shown, but it is a line connecting [0, 0] and $[A_o, B_o]$ and above the points generated by using (20). This result suggests that the mixing within the 2-D model produces a broader $G_o(T)$ value than the HP analytic model. This is not hard to imagine when we realize that there must be an age spectrum offset, as seen in Figure 2b, which is not included in (8). This offset is due to the general advection of parcels to the sample location as seen in Figure 2a. In addition, there is large-scale overturning within the 2-D model, and old polar vortex air mixing with young tropical air will create a broader age spectrum than that defined by (8).

In general, for a given function $G_o(T)$ the sample trace gas amounts must lie between the SPPC and the limit chord. The above results suggest that the limit chord is not restrictive enough and the PK limit is probably a more realistic upper bound. The fact that mixing produces chords which connect parts of the tracer-tracer correlation curve has also been pointed out by *Waugh et al.* [1997a] and *Thuburn and McIntyre* [1997] to explain mixing between discreet air masses. Here we further argue that such mixing, as characterized by the changing age spectrum as a function of season, is continuously forming and reforming points along different chords which are bounded by the SPPC.

There is clearly information about the range of mixing in the curvature of the tracer-tracer correlation. As pointed out by *Holton* [1986] and *Mahlman et al.* [1986], the stratospheric overturning circulation along with photochemistry will maintain the tracer gradients against the effect of isentropic mixing. Each isentropic level then defines a chord with a slightly different slope. This explains why even in a fairly well-mixed system, the tracer-tracer correlation line will be slightly curved and why the curve can be seen as a series of points lying on interlocking chords when the data is analyzed on isentropic surfaces (A. Dessler, private communication, 1998).

Plate 5 shows N_2O sample values plotted against CFC-11 sample values. The samples are generated by averaging the trajectory model data shown in Figure 5 within 10° by 2 km regions. As expected, most of the model sample points fall between a line defined by the PK limit and the Lagrangian parcel curve. Overplotted on Plate 5 are the data from Atmospheric Laboratory for Applications and Science (ATLAS) missions 1–3 Atmospheric Trace Molecule Spectroscopy (ATMOS) instrument [*Gunson et al.*, 1996]. The ATLAS flights took place March 24 to April 3, 1992; April 8–16, 1993; and November 3–14, 1994, and the ATMOS instrument acquires high-resolution infrared solar absorption spectra from which constituent profiles are retrieved. The high quality of this data set makes if useful for correlations over a wide range in CFC-11 and N_2O values. The profiles obtained by ATMOS 3 have been validated by nearby ER-2 measurements [*Chang et al.*, 1996a, b].

The comparison between the ATMOS and 2-D model data is good, although there appears to more of the ATMOS data along the PK-limit line than generated using the trajectory 2-D model for high values of CFC-11 and N_2O. The likely explanation for the discrepancy is a difference in the sample size between the numerical calculation and the observations. In other words, the trajectory model has not adequately characterized the age spectrum in the high N_2O–CFC-11 region due to too few parcels. For low values of N_2O and CFC-11 the size of the scatter in the ATMOS and model points is about the same and the data falls off the PK limit as older air parcels dominate $G_o(T)$.

5. Summary and Discussion

The purpose of this paper is to present a Lagrangian interpretation of the mixing of chemically active trace gases. The methodology developed extends the age-of-air formalism of HP in which a "sample" of air is defined as a collection of irreducible parcels. The age of each of the irreducible parcels is clocked from their tropopause crossing time, and the age spectrum is the normalized PDF of parcel ages within the sample. Because the parcels are irreducible, mixing along the parcel path does not take place, but the effects of mixing are included in the sampling of a large number of parcels. The tracer spectrum is defined as the PDF of the tracer ratio to the tracer amount at the tropopause.

Photochemical exposure, as opposed to age, is the actual clock that determines the tracer amounts for the individual parcels. For long-lived tracers the photolysis rates are generally scalable so that there is a high degree of correlation between the trace gas amounts computed for individual parcels. On a tracer-tracer diagram this means that the irreducible parcels form a very tight curve, which we refer to as the single-path photochemistry curve (SPPC). As they move through the stratosphere, we can think of parcels moving along the SPPC, with different parcels moving at different rates. Since the sample consists of an ensemble of parcels at different points along the SPPC, the sample point must lie on the interior of the SPPC.

In order to infer transport related quantities such as mean age from trace gas measurements we must connect age and photochemical exposure. We find that the variations in photochemical exposure tend to average to zero for parcels with similar ages. Thus, for an ensemble of parcels in the sample with the same age the photochemical exposure can be computed using the average path. This is called the average path approximation (APA). This approximation allows us to interpret the age spectrum as a "weight" which gives the relative

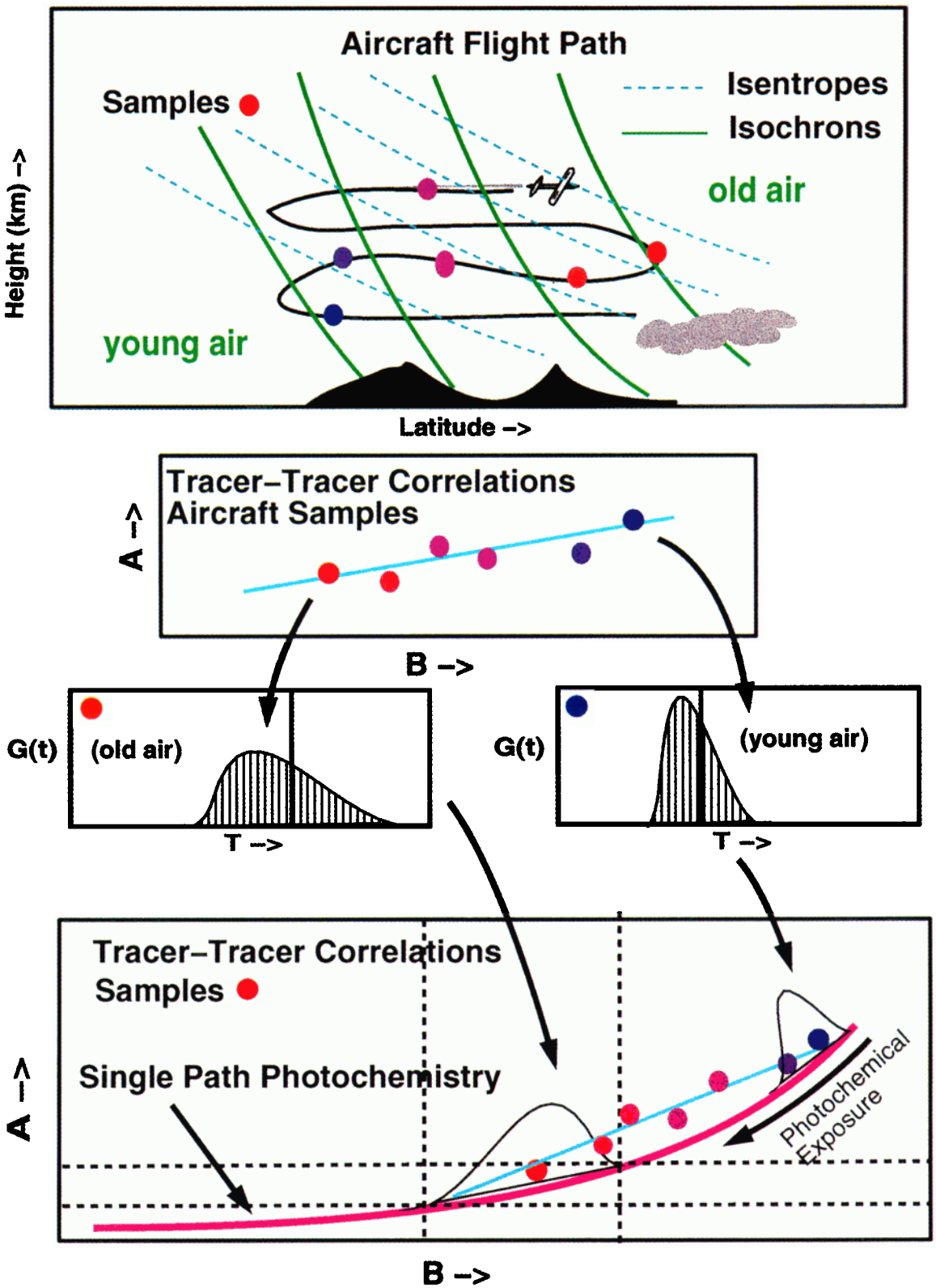

Plate 4. A cartoon that shows our interpretation of trace gas measurements. (top) An aircraft collecting samples of air indicated by colored dots. The green lines are equal mean age contours, or isochrons; the blue lines are constant potential surfaces or isentropes. The color of the dot indicates the mean age, with blue indicating young air and red indicating old air. (top middle) Sample values of trace gases A and B plotted against each other. The data fit is the light blue line. (bottom middle) Age spectrum $G(t)$ plotted for two of the samples. (bottom) Age spectrum for the old and young samples formed from the weighting of points on the single-path photochemistry curve. As irreducible parcels move through the stratosphere, they travel down the single-path photochemistry curve as their photochemical exposure increases.

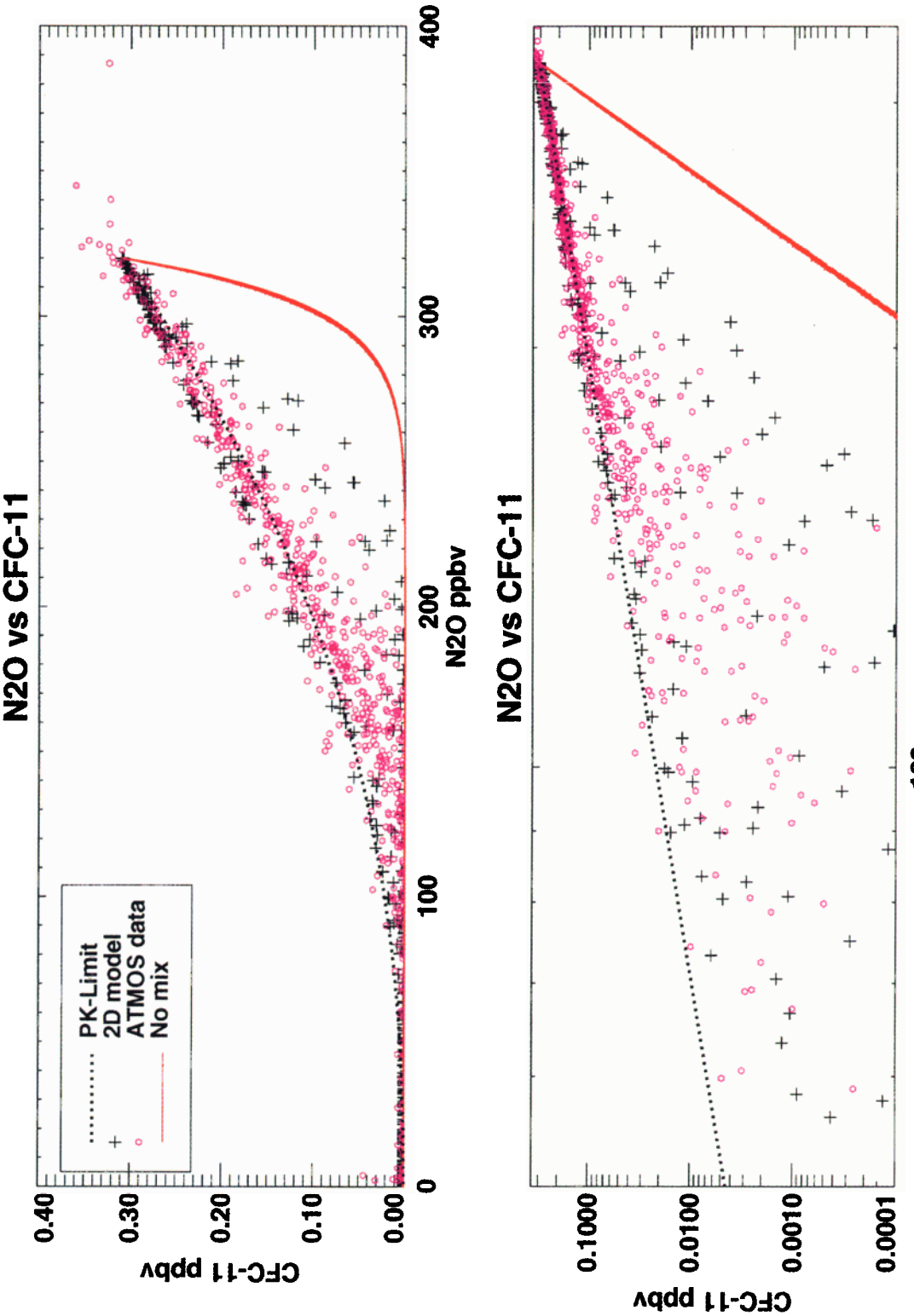

Plate 5. As in Figure 5, the Lagrangian points (red line), and data from samples within 10° by 2 km region centered on the 2-D model grid (crosses). ATMOS measurements (pink circles) from the ATLAS 1–3 missions are also shown. The PK limit for the 2-D model is the dashed line (see Figure 5). The 2-D model data falls between the single-path photochemistry limit and the PK limit as expected. The ATMOS data are not constrained to tropospheric values of N_2O or CFC-11 so may fall above the PK-limit curve.

contribution of equivalent parcels with different ages. The age spectrum can then be converted into a tracer spectrum using the photochemistry along the average path for all the parcels that have the same age. Using a 2-D model, we show that these approximations work quite well for N_2O and CFC-11 [see also *Volk et al.*, 1997].

Because photochemical loss depends mainly on the parcel age, we can interpret the age spectrum as a kind of weighting function for the SPPC in the tracer-tracer correlation curve. Analytical examples which form tracer-tracer correlation curves show that these curves tend to be linear on log-log plots, a result first derived by *Plumb and Ko* [1992], but this is shown not to be true in general. Using the lifetime of tracers in the 2-D model, we find that N_2O and CFC-11 data from the 2-D model data and from the ATMOS instrument appear to fall between the limit curves formed from the tracer lifetime limit and SPPC limit.

The extension of the age-of-air formalism to chemically active trace gases allows the possibility of gaining more information on the age spectrum than can be gained from the study of inert tracers alone. Shorter-lived tracers are sensitive to younger parts of the age spectrum, while the inert tracers are sensitive to the whole spectrum. The basic method would be to use (17) given the tracer measurement and an estimate of the path integrated loss rate as a function of age. From each tracer measurement, assuming different loss rates, one new piece of information about the age spectrum would then be obtained. Because the path-integrated 2-D model loss rates appear to be a relatively smooth function of age and position for most long lived tracers, it may be possible to use the 2-D model loss rates and actual observations to derive information about the atmospheric age spectrum.

Finally, the connection between the age and tracer spectrum suggests a strong coupling between the mean age diagnostic and the long-lived tracer fields. However, the long-lived tracer distribution is not sensitive to the tail of the age spectrum, while the mean age is very sensitive to the tail; thus the mean age can be a misleading diagnostic. For example, the trace gas distribution in a model might be quite unrealistic while the mean age field is very realistic and vice versa. This can happen because of the strong weight that old air parcels give to computing the mean age. At the same time the old air parcels give almost no weight to computing the tracer amount for the long-lived tracers. Thus strong emphasis should not be placed on the mean age as a diagnostic determining the success or failure of a model transport scheme especially in regions where old air parcels are a significant component of the sample (e.g., winter polar regions).

Acknowledgments. The authors would like to acknowledge helpful comments on an early draft of this paper by Tim Hall and the extensive comments by one of the reviewers. This work was supported by NASA's Earth Science Enterprise's EOS Interdisciplinary Science Program.

References

Bischof, W., R. Borchers, P. Fabian, and B. C. Krueger, Increased concentration and vertical distribution of carbon dioxide in the stratosphere, *Nature*, *316*, 708–710, 1985.

Boering, K. A., S. C. Wofsy, B. C. Daube, H. R. Schneider, M. Loewenstein, and J. R. Podolske, Stratospheric transport rates and mean age distributions derived from observations of atmospheric CO_2 and N_2O, *Science*, *274*, 1340–1343, 1996.

Chang, A. Y., et al., A comparison of measurements from ATMOS instruments aboard the ER-2 aircraft: Halogenated gases, *Geophys. Res. Lett.*, *23*, 2393–2396, 1996a.

Chang, A. Y., et al., A comparison of measurements from ATMOS instruments aboard the ER-2 aircraft: Tracers of atmospheric transport, *Geophys. Res. Lett.*, *23*, 2389–2392, 1996b.

Daniel, J. S., S. M. Schauffler, W. H. Pollock, S. Solomon, A. Weaver, L. E. Heidt, R. R. Garcia, E. L. Atlas, and J. F. Vedder, On the age of stratospheric air and inorganic chlorine and bromine release, *J. Geophys. Res.*, *101*, 16,757–16,770, 1996.

DeMore, W. B., et al., Chemical kinetics and photochemical data for use in stratospheric modeling, *JPL Publ.*, *94–26*, 1994.

Elkins, J. W., et al., Airborne gas chromatograph for in situ measurements of long-lived species in the upper troposphere and lower stratosphere, *Geophys. Res. Lett.*, *23*, 347–350, 16,770, 1996.

Feller, W., *An Introduction to Probability Theory and Its Applications*, vol. 1, John Wiley, New York, 1968.

Fleming, E. L., C. H. Jackman, R. S. Stolarski, and D. B. Considine, Simulation of stratospheric tracers using an improved empirically based model transport formulation *J. Geophys. Res.*, *104*, 23,911–23,934, 1999.

Gunson, M. R., et al., The atmospheric trace molecule spectroscopy (ATMOS) experiment: Deployment on the ATLAS space shuttle missions, *Geophys. Res. Lett.*, *23*, 2333–2336, 1996.

Hall, T. M., and R. A. Plumb, Age as a diagnostic of stratospheric transport, *J. Geophys. Res.*, *99*, 1059–1070, 1994.

Hall, T. M., and D. W. Waugh, Timescales for the stratospheric circulation derived from tracers, *J. Geophys. Res.*, *102*, 8991–9001, 1997.

Hall, T. M., and D. W. Waugh, The influence of nonlocal chemistry on tracer distributions: Inferring the mean age of air from SF_6, *J. Geophys. Res.*, *103*, 13,327–13,336, 1998.

Hall, T. M., D. W. Waugh, K. A. Boering, and R. A. Plumb, Evaluation of transport in stratospheric models, *J. Geophys. Res.*, *104*, 18,815–18,839, 1999.

Harnisch, J., R. Borchers, P. Fabian, and M. Maiss, Tropospheric trends for CF_4 and C_2F_6 since 1982 derived from SF_6 dated stratospheric air, *Geophys. Res. Lett.*, *23*, 1099–1102, 1996.

Holton, J. R., A dynamically based transport parameterization for one-dimensional photochemical models of the stratosphere, *J. Geophys. Res.*, *91*, 2681–2686, 1986.

Holton, J. R., P. H. Haynes, M. E. McIntyre, A. R. Douglass, R. B. Rood, and L. Pfister, Stratosphere-troposphere exchange, *Rev. Geophys.*, *33*, 403–439, 1995.

Jackman, C. H., E. L. Fleming, S. Chandra, D. B. Considine, and J. E. Rosenfield, Past, present, and future modeled ozone trends with comparisons to observed trends, *J. Geophys. Res.*, *101*, 28,753–28,767, 1996.

Kida, H., General circulation of air parcels and transport characteristics derived from a hemispheric GCM, part 2, Very long-term motions of air parcels in the troposphere and stratosphere, *J. Meteorol. Soc. Jpn.*, *61*, 510–522, 1983.

Mahlman, J. D., H. Levy II, and W. J. Moxim, Three-dimensional simulations for stratospheric N_2O: Predictions for other trace constituents, *J. Geophys. Res.*, *91*, 2687–2707, 1986.

McIntyre, M. E., Atmospheric dynamics: Some fundamentals, with observational implications, in *The Use of EOS for the Study of Atmospheric Physics*, edited by G. Visconti and J. Gille, *Proc. Int. Sch. Phys. "Enrico Fermi"*, *115*, 313–386, 1992.

Patra, P. K., S. Lal, B. H. Subbaraya, C. H. Jackman, and P. Rajaratnam, Observed vertical profile of sulfur hexafluoride (SF_6) and its atmospheric applications, *J. Geophys. Res.*, *102*, 8855–8859, 1997.

Plumb, R. A., A "tropical pipe" model of stratospheric transport, *J. Geophys. Res.*, *101*, 3957–3972, 1996.

Plumb, R. A., and M. K. W. Ko, Interrelationships between mixing ratios of long-lived stratospheric constituents, *J. Geophys. Res.*, *97*, 10,145–10,156, 1992.

Plumb, R. A., and D. D. McConalogue, On the meridional structure of long-lived tropospheric constituents, *J. Geophys. Res.*, *93*, 15,897–15,913, 1988.

Schmidt, U., and A. Khedim, In situ measurements of carbon dioxide in the winter arctic vortex and at midlatitudes: An indicator of the "age" of stratospheric air, *Geophys. Res. Lett.*, *18*, 763–766, 1991.

Schoeberl, M. R., and L. Sparling, Trajectory modeling, in *Diagnostic Tools in Atmospheric Physics*, edited by G. Fiocco and G. Visconti, *Proc. Int. Sch. Phys.* "Enrico Fermi," *124*, 289–306, 1995.

Thuburn J., and M. E. McIntyre, Numerical advection schemes, cross-isentropic random walks, and correlations between chemical species, *J. Geophys. Res.*, *102*, 6775–6796, 1997.

Volk, C. M., J. W. Elkins, D. W. Fahey, G. S. Dutton, J. M. Gilligan, M. Loewenstein, J. R. Podolske, K. R. Chan, and M. R. Gunson, Evaluation of source gas lifetimes from stratospheric observations, *J. Geophys. Res.*, *102*, 25,543–25,564, 1997.

Waugh, D. W., et al., Mixing of polar vortex air into middle latitudes as revealed by tracer-tracer scatterplots, *J. Geophys. Res.*, *102*, 13,119–13,134, 1997a.

Waugh, D. W., et al., Three-dimensional simulations of long-lived tracers using winds from MACCM2, *J. Geophys. Res.*, *102*, 21,493–21,513, 1997b.

E. L. Fleming, C. H. Jackman, M. R. Schoeberl, and L. C. Sparling, NASA Goddard Space Flight Center, Code 916, Greenbelt, MD 20771. (jackman@assess.gsfc.nasa.gov; schom@zephyr.gsfc.nasa.gov; sparling@dynarama.gsfc.nasa.gov)

(Received December 31, 1998; revised July 19, 1999; accepted July 26, 1999.)